Application of Mean-Motion-Based Artificial Potentials for a Cluster Flight Mission Scenario

Federico Fumenti, David Seelbinder and Stephan Theil

Abstract Cluster flight is one of the key technologies that are required to enable the deployment of distributed space systems. Through the concept of cluster flight, a large monolithic structure can be replaced with multiple smaller spacecraft, permitting to overcome physical limitations and improve mission performance. To ensure a safe relative motion between several objects that fly in proximity, the guidance and control algorithm must be designed in order to be scalable, autonomous, and responsive. A technique to meet these requirements by employing the method of the artificial potentials is presented in this paper. For a cluster of spacecraft that are distributed in the along-track direction in a leader-follower manner, the relative distances can be altered by focusing and adjusting the mean motion of the spacecraft. An artificial-potential-based approach can be used to evaluate corrections of the semi-major axes by only reacting on the current configuration, with no need to perform trajectory predictions.

1 Introduction

Over the last two decades the idea of deploying a cluster of objects that fly in proximity gained much popularity thanks to the benefits that it could offer; especially if it is considered as an alternative to the use of a single large structure. The mission could profit in several ways from a fractionated architecture: flexibility and redundancy could be augmented, costs and risks could be reduced, physical limitations like launch mass or launch volume could be overcome. One of the main challenges that stand in the way of the implementation of the cluster concept, is the availability of guidance and control algorithms that can ensure a safe relative motion between the objects of the cluster. In the field of formation flight relative motion is already

Federico Fumenti, David Seelbinder, Stephan Theil

DLR, Institute of Space Systems, Robert Hooke Str. 7, 28359, Bremen

e-mail: `federico.fumenti@dlr.de`

widely investigated. The spacecraft in a formation are usually required to maintain a precise relative geometry, with the consequence that the relative distances are allowed to vary in narrow ranges with respect to nominal values. In a cluster, on the other hand, only minimum and maximum distance constraints (DC) are imposed, to prevent modules from drifting away or from colliding. The different control effort in the two scenarios is self-evident, and for this reason the attention of researchers started to be drawn towards the design of long-term passive distance-bounded orbits (see e.g., [3, 12, 13, 17, 18, 20]), as well as towards new cluster-based approaches to perform orbital corrections aimed at satisfying the distance requirements (see e.g., [7, 10, 19, 20]).

To correctly deal with multiple objects and their relative motion, the employed algorithms must be highly responsive and able to work autonomously, such that the safety of the cluster does not entirely depend on the ground stations. A powerful tool that presents the desired features of autonomy and responsiveness and that is already largely used to study problems involving relative motion between several objects, is the method of the artificial potential fields (APF). Through the definition of attractive and repulsive behaviors, this method can enforce obstacle avoidance and steer the system towards a goal configuration, by only reacting on the current positions. In the space domain the APF method has many potential applications, such as rendezvous maneuvers [2, 11], or (re-)configuration of multiple spacecraft [8, 9, 15, 16], but its use is still significantly limited, due to the complexity of the equations of motion that describe orbital-mechanics-based problems. Space research involving this method is nowadays restricted to small-sized relative motion problems, in which the simplified Hill-Clohessy-Wiltshire model could be used.

For the work presented in this paper the APF method has been applied to the cluster keeping problem, and a control technique is proposed to evaluate the orbital corrections that are required by the spacecraft to keep their relative distance constraints satisfied. Both small- and large- sized clusters are considered, leading to the need for dropping distance-related simplified assumptions and developing a general cluster keeping approach.

The paper opens with the problem statement, which is introduced in Section 2. Section 3 presents the APF method and describes its application to the cluster keeping problem. Mission scenarios used to test the proposed technique are briefly outlined in Section 4. Section 5 presents a sample case scenario to show the application of the method. Section 6 reports the results of the numerical simulations and discusses the method performance. Section 7 finally summarizes the conclusions.

2 Problem Statement

For the problem of the cluster keeping treated in this paper, a group of N spacecraft flying in proximity in a low Earth orbit (LEO) scenario is considered. The initial distribution of the spacecraft is assumed to be obtained from the technique of the delayed elements, which has been originally described by De Bruijn and Gill [3]

and resembles a leader-follower distribution, as the spacecraft are arranged in the along-track direction. The along-track direction is defined in the local-vertical-local-horizontal (LVLH) frame. This reference frame is typically used in coordinated-flight-based problems to better show the relative motion with respect to a reference point (RP). The origin of the frame is placed in the reference point, the xy-plane is coincident with its orbital plane, and the x-axis is parallel to its position vector (positive outwards). The radial, along-track, and cross-track directions are defined by the x-, y-, and z-axis.

Given a lower boundary D_{min} and an upper boundary D_{max} for the relative distances, the selected configuration technique permits to identify relative orbits that are invariant to the perturbations and that naturally satisfy the desired DC. Consider a spacecraft A, a reference time t_0, and a 6x1 vector $\boldsymbol{\text{œ}}(t_0)$ of classical Keplerian elements that expresses the state of A at t_0. The vector $\boldsymbol{\text{œ}}$ is defined as $\boldsymbol{\text{œ}} = (a\ e\ i\ \Omega\ \omega\ M)^T$, where a is the semi-major axis, e the eccentricity, i the inclination, Ω the right ascension of the ascending node (RAAN), ω the argument of perigee, and M the mean anomaly. The distance between A and a second spacecraft B can remain bounded over time if the initial state of B is defined as

$$\boldsymbol{\text{œ}}_B(t_0) = \boldsymbol{\text{œ}}_A(t_0) + \int_{t_0}^{t_0+\tau} \dot{\boldsymbol{\text{œ}}}_A dt \tag{1}$$

where $\dot{\boldsymbol{\text{œ}}}_A$ denotes the rates of the orbital elements of A, and τ represents the time delay between the passage of A and B through the same positions. As this work focuses on spacecraft in LEO, the rates $\dot{\boldsymbol{\text{œ}}}$ take the gravitational potential, as well as the drag, into account.

For a cluster of N objects, the design process has to deal with $N_p = 0.5N(N-1)$ pairs of spacecraft, thus the management of the distance constraints can become extremely complex as N grows. The conducted work, however, could benefit from several simplifications that derive from the along-track distribution of the spacecraft. First of all, by exploiting Kepler's second law and by approximating the distance d between A and B with the arc of trajectory traveled in τ, a correspondence between separation distance d and time difference τ can be identified

$$\mathcal{T} : d \to \tau. \tag{2}$$

Equation (2) permits to transform the distance boundaries $[D_{min}\ D_{max}]$ into time boundaries $[\tau_{min}\ \tau_{max}]$, leading to an orbit design that is based on a scalar parameter $|\tau| \in [\tau_{min}\ \tau_{max}]$. The use of the absolute value $|\tau|$ derives from the fact that the time difference τ can be positive or negative depending on whether B is located in front of or behind A in the along-track direction.

A second simplification can be obtained by using a reference point to define the center of the cluster and to design the initial states of all the spacecraft through Eq. (1). In this way, the initial configuration problem consists in identifying the delay τ for each object, and can be simplified considering that the minimum distance constraints need to be satisfied only for neighboring spacecraft, whilst the maximum distance constraints only between the spacecraft and the center of the cluster. For

a better understanding, consider the sample scenario given in Fig. 1. The cluster
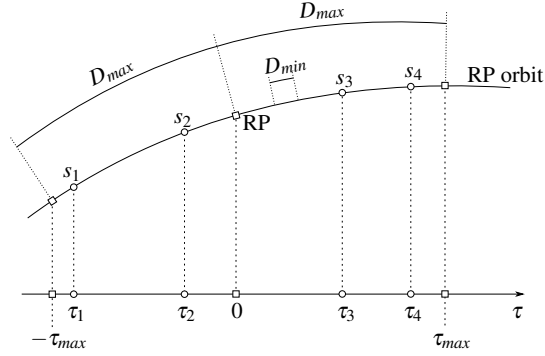
Fig. 1: Sample scenario with $N = 4$ spacecraft and their distribution in a 1-D space.

counts $N = 4$ satellites s_i, for $i = 1, 2, ..., N$, and is centered on a reference point RP, where the origin of the τ reference frame ($\tau = 0$) is set. Given two generic objects $[s_i\ s_j]$, the distance constraints

$$d_i < D_{max} \tag{3}$$

$$d_j < D_{max} \tag{4}$$

$$d_{i/j} > D_{min} \tag{5}$$

can be expressed in the one-dimensional space as

$$|\tau_i| < \tau_{max} \tag{6}$$

$$|\tau_j| < \tau_{max} \tag{7}$$

$$|\tau_{i/j}| > \tau_{min}, \tag{8}$$

where d_i and d_j are the distances of s_i and s_j from the RP, $d_{i/j}$ the distance between s_i and s_j, τ_i and τ_j are the time differences between s_i and the RP and between s_j and the RP, and $\tau_{i/j}$ is the time difference between s_i and s_j.

An initial configuration defined by satisfying Eqs. (6) to (8) complies with the desired DC at the initial time, but might still need orbital corrections at future times $t > t_0$. With reference to the invariance to perturbations of the relative orbits that derives from the use of Eq. (1), the validity of this condition might require additional constraints, depending on the involved perturbations. For example, when the gravitational potential is taken into account the invariance is guaranteed with no limitations, but in the presence of the drag it requires the spacecraft to have the same ballistic coefficient. Since it is unlikely that this requirement is satisfied by all the objects of a cluster, for the considered scenario the application of Eq. (1) can still greatly reduce the differential perturbations, but over time a slow drift of the relative distances should be expected and cluster keeping strategies should be implemented.

In addition, since the reference point is not influenced by the atmospheric drag, it does not experience the orbital decay that affects the spacecraft. As a result the spacecraft drift from the RP and over time require corrective maneuvers to remain close to it. This difference could be removed by including a fictitious drag effect also on the evolution of the reference point, but by adjusting the motion of the spacecraft to follow the ideal RP, the orbital decay of the entire cluster is already counteracted.

Two satellites that are initialized through the technique of the delayed elements have the same mean motion and keep their distance approximately constant over time (small drift derive from the atmospheric drag, as previously explained). One simple way to alter their distance is by providing a differential semi-major axis, since the resultant differential mean motion would cause one satellite to move faster than the other. A positive distance rate, for example, can be obtained by lowering the orbit of the front satellite and/or raising the orbit of the rear satellite; a negative distance rate, on the contrary, requires that the rear satellite is moved into a lower orbit and/or that the front satellite is moved into a higher orbit (the terms *front* and *rear* refer to the position of the satellites in the along-track direction). Also, the larger the differential semi-major axis, the larger the differential mean motion and the faster the distance change between the objects for a given time interval.

The cluster keeping technique proposed in this work aims at controlling the along-track distances between the spacecraft by changing their semi-major axes, which in turn alter their mean motions. The required changes are evaluated by exploiting the method of the artificial potentials, as described in the next section.

3 APF-based Cluster Keeping

For the introduction of the artificial potentials technique, a group of N objects that move in a p-dimensional Euclidean space can be considered. The motion of the generic i-th object is influenced by the others according to

$$\dot{\mathbf{x}}_i = \sum_{j=1, j\neq i}^{N} F(\mathbf{x}_i - \mathbf{x}_j), \tag{9}$$

where $\mathbf{x}_i \in \mathbb{R}^p$ is the position vector of the object, $\dot{\mathbf{x}}_i$ is its velocity vector, and F is a function that represents its interaction with the other objects. Given a mathematically differentiable function U that can be conceptually associated with the energy of the system, by employing its negative gradient as function F, the system can be steered towards a less energetic configuration. The design of the potential U, or equivalently of the function F, consists in identifying proper expressions for these functions, such that the least energetic configuration is also the desired configuration. In general, the function U and F are composed of two terms

$$\begin{aligned} U &= U_A + U_R \\ F &= -\nabla U = -\nabla U_A - \nabla U_R = F_A + F_R, \end{aligned} \tag{10}$$

that represent an attractive and a repulsive behaviour, and can be distinguished by the subscripts A and R, respectively. The first term allows the aggregation of the objects, the second prevents collisions between them. A further insight into the APF technique and the properties of the functions U and F can be found, e.g., in [5, 6].

In this work, the peculiar distribution of the spacecraft permits to approximate their distance d with their along-track separation $|\Delta y|$

$$d \approx |\Delta y|, \tag{11}$$

where Δy is their relative position in the along-track direction. This means that the scalar variable y replaces the vectorial variable $\mathbf{x}$ in Eq. (9), and that the problem can be studied in a one-dimensional space. Equation (9) can then be transformed into

$$\dot{y}_i = F_A(\Delta y_i) + \sum_{j=1, j \neq i}^{N} F_R(\Delta y_{i/j}), \tag{12}$$

where Δy_i is the relative along-track position of i with respect to the RP, and $\Delta y_{i/j}$ is the relative along-track position of i with respect to j. Note that $\Delta y_i = y_i$, since the RP is located at $y = 0$. As it can be seen, the total artificial force that influences the motion of the generic object i has only one attractive contribution, but $N-1$ repulsive ones. This trivially derives from the use of the reference point to identify the center of the cluster. To prevent an object from drifting away, it is sufficient to limit its distance from the center, thus the attractive contribution only needs to depend on the separation $|y_i|$. On the contrary, the object i could theoretically collide with any other object j, thus the repulsive force must consist of $N-1$ contributions.

The attraction and the repulsion have been modeled such that the generated artificial forces have a distance-dependent magnitude that increases monotonically as the distances approach their boundary values. To obtain this behaviour, the attractive and repulsive contributions U_A and U_R have been built upon exponential terms as

$$U_A = k_{1,A} \left(e^{-k_{2,A}|\Delta y|} + e^{k_{2,A}|\Delta y|} \right) \tag{13}$$

$$U_R = k_{1,R} \frac{e^{-k_{2,R}|\Delta y|}}{\Delta y^2}, \tag{14}$$

leading in turn to the following expressions for the negative gradients F_A and F_R

$$F_A = -\nabla U_A = k_{1,A} k_{2,A} \frac{\Delta y}{|\Delta y|} \left(e^{-k_{2,A}|\Delta y|} - e^{k_{2,A}|\Delta y|} \right) \tag{15}$$

$$F_R = -\nabla U_R = k_{1,R} \frac{e^{-k_{2,R}|\Delta y|}}{\Delta y^3} \left(2 + k_{2,R}|\Delta y| \right), \tag{16}$$

where the coefficients $k_{1,A}$, $k_{2,A}$, $k_{1,R}$, and $k_{2,R}$, are tuning parameters. Figure 2 shows the shape of the functions U and F. Note that this is only a qualitative representation of the four functions. In Figs. 2a and 2c, the origin of the frame $\Delta y = 0$ represents the location of the reference point, while in Figs. 2b and 2d it refers to the location

(a) Attractive potential.

(b) Repulsive potential.

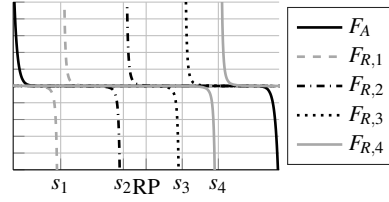(c) Attractive function.

(d) Repulsive function.
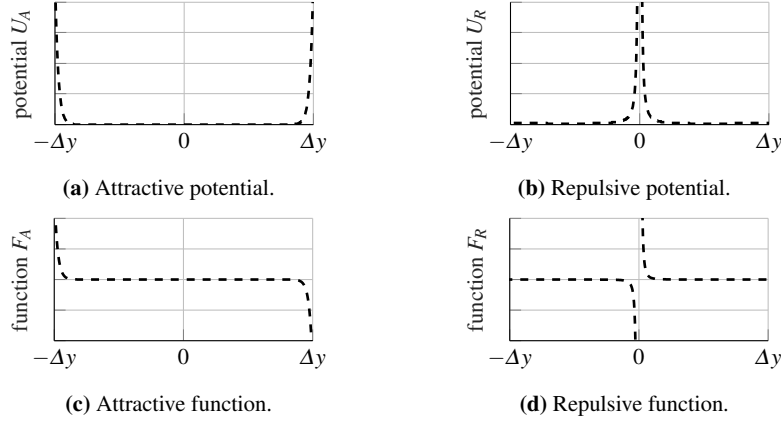
Fig. 2: Representation of the U and F functions.

of the object j with respect to which the object i of interest computes its reaction. For example, for the configuration shown in Fig. 1, the attractive and repulsive contributions of the functions U and F are given in Figs. 3 and 4. In Fig. 3, the term
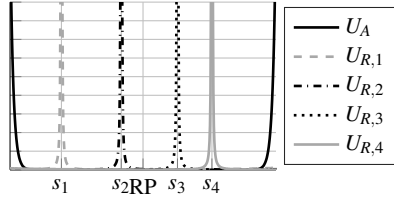
Fig. 3: Potentials U for a sample scenario with $N = 4$ spacecraft.

Fig. 4: Functions F for a sample scenario with $N = 4$ spacecraft.

U_A refers to the attraction to the center, while the term $U_{R,i}$ represents the repulsion associated with the spacecraft s_i. The same notation is used in Fig. 4 for the contributions to the function F.

To connect the APF method and the U and F functions with the cluster keeping problem and the control of the relative distances, consider a simple 1-D problem with two objects A and B separated by a distance d, moving at the same speed, and with one chasing the other. A variation of the distance Δd in a time interval Δt can be interpreted as the relative velocity between the objects and can be obtained by providing a $\Delta v = \frac{\Delta d}{\Delta t}$ to one of the objects (the direction of the application and the recipient object determines the sign of the distance variation). This simple situation represents an approximation of what happens in the scenario treated in this work, with a cluster of spacecraft distributed in a leader-follower fashion. Given two objects with differential mean motion Δn, within a time interval Δt their mean anomaly separation changes by an amount $\Delta M = \Delta n \Delta t$, with a corresponding distance separation $d \approx a \Delta M$. From the combination of these equations, a relationship

between the distance rate $\dot{d}$ and the differential mean motion can be obtained as

$$\dot{d} = a\Delta n, \tag{17}$$

and since the term $\dot{d}$ is provided by Eq. (12), Eq. (17) can be used to evaluate the differential mean motion Δn. Eventually, the semi-major axis difference can be recovered from the definition of the differential mean motion

$$\Delta n = \sqrt{\frac{\mu}{(a+\Delta a)^3}} - \sqrt{\frac{\mu}{a}}, \tag{18}$$

where μ is the gravitational parameter of the Earth.

The equivalence between the distance rate $\dot{d}$ and the Δv impulse is the basis for the tuning process. In general, since four coefficients need to be determined $(k_{1,A}, k_{2,A}, k_{1,R}, k_{2,R})$, the problem requires four boundary conditions

$$\begin{cases} F_{A,1} = F_A(\Delta y = |\Delta y_{1,A}|) & \text{(19a)} \\ F_{A,2} = F_A(\Delta y = |\Delta y_{2,A}|) & \text{(19b)} \\ F_{R,1} = F_R(\Delta y = |\Delta y_{1,R}|) & \text{(19c)} \\ F_{R,2} = F_R(\Delta y = |\Delta y_{2,R}|), & \text{(19d)} \end{cases}$$

where the terms $F_{A,1}$, $F_{A,2}$, $F_{R,1}$, and $F_{R,2}$, denote known values of the functions F_A and F_R at $|\Delta y_{1,A}|$, $|\Delta y_{2,A}|$, $|\Delta y_{1,R}|$, and $|\Delta y_{2,R}|$. For example, it can be assumed that the functions F are negligible at distances very far from the boundaries

$$\min(|F_A|) = |F_A(\Delta y = 0)| \approx 0 \tag{20}$$

$$\min(|F_R|) = |F_R(|\Delta y| = 2D_{max})| \approx 0 \tag{21}$$

and have their maximum magnitude in correspondence of the distance boundaries

$$\max(|F_A|) = |F_A(|\Delta y| = D_{max})| \tag{22}$$

$$\max(|F_R|) = |F_R(|\Delta y| = D_{min})|. \tag{23}$$

To perform realistic simulations, however, a minimum providable Δv related to the minimum impulse bit of the spacecraft propulsion system can be used, thus Eqs. (20) and (21) can be replaced with

$$\min(|F_A|) = |F_A(|\Delta y_A^*|)| \tag{24}$$

$$\min(|F_R|) = |F_R(|\Delta y_R^*|)|, \tag{25}$$

where the parameters Δy^* denote the distances at which the functions F assume the minimum value. For the maximum values instead, it does not make sense to refer to the maximum providable Δv, because the propulsion system can be activated and fire for long time intervals. The determination of the upper boundary for the

functions F becomes then a part of the tuning process and is selected as the minimum value that can ensure the satisfaction of the constraint $\beta = \frac{|F_{max}|}{|F_{min}|} > 1$, where $F_{max} = \max(|F_A|) = \max(|F_R|)$ and $F_{min} = \min(|F_A|) = \min(|F_R|)$.

To obtain a control scheme that involves sparse maneuvers and does not require the spacecraft to perform corrections continuously, the values y_A^* and y_R^* are chosen close to the distance boundaries. Consider the sample scenario given in Fig. 1 and suppose that at a given time t the spacecraft are equally spaced as pictured in Fig. 5 with the relative distance d_{eq} given by
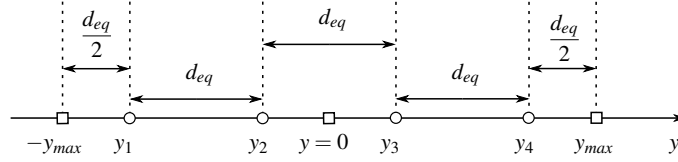
Fig. 5: Sample scenario of $N = 4$ equally spaced spacecraft.

$$d_{eq} = \frac{2D_{max}}{N}. \tag{26}$$

This configuration represents an equilibrium for the cluster and no spacecraft are supposed to maneuver. This means that to avoid continuous corrections it is required to tune the potentials by choosing $|\Delta y_A^*| > \frac{d_{eq}}{2}$ and $|\Delta y_R^*| < d_{eq}$, so that the spacecraft motion can be influenced only in proximity of the high potential regions.

Figure 6 gives a qualitative representation of the attractive potential U_A (it would correspond to Fig. 2a, but for simplicity only the right branch is shown). Together
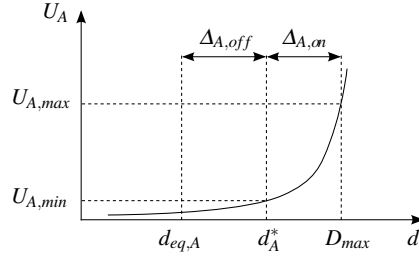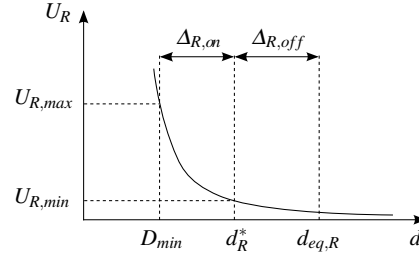

Fig. 6: Tuning of the attraction.

Fig. 7: Tuning of the repulsion.

with the distance boundary D_{max}, the figure includes also the distance d_A^*, which represents the separation $|y_A^*|$, and the distance $d_{eq,A}$, which is defined as

$$d_{eq,A} = D_{max} - \frac{d_{eq}}{2}, \tag{27}$$

and represents the attractive-equilibrium distance, i.e. the distance between the two most external spacecraft and the center of the cluster when the spacecraft are equally spaced. With reference to Fig. 5 for example, the $d_{eq,A}$ would be associated with the objects n.1 and n.4. Since the function F must be equal to F_{min} for $d = d_A^*$ and

negligible for $d = d_{eq,A}$, it must hold $d_{eq,A} < d_A^*$, and the selection of

$$d_A^* = d_{eq,A} + \alpha_A(D_{max} - d_{eq,A}) \tag{28}$$

with $0 < \alpha_A < 1$ is the key for preventing the control from being constantly on. The larger the parameter α_A, the wider the region of inactivity $\Delta_{A,off} = d_A^* - d_{eq,A}$. On the other hand, a large α_A involves a steep attractive potential U_A, with the consequence that the force F_A grows quickly from its minimum to its maximum value. As opposite to the region of inactivity, a region of activity with width $\Delta_{A,on}$ can be identified as the range of distances that provide a non-negligible contribution F_A.

In a similar way, Fig. 7 can be considered for the repulsive potential, with the repulsive-equilibrium distance $d_{eq,R}$ defined as

$$d_{eq,R} = d_{eq}. \tag{29}$$

The region of inactivity has a width $\Delta_{R,off} = d_{eq,R} - d_R^*$, for which it holds

$$d_R^* = D_{min} + \alpha_R(d_{eq,R} - D_{min}) \tag{30}$$

with $0 < \alpha_R < 1$. Note that the effects of α_R and α_A are opposed, since the larger the α_R, the smaller the region of inactivity $\Delta_{R,off}$.

An insight into the behaviour that is tried to be achieved through the application of the APF technique is given in Fig. 8. A group of four objects moving in a
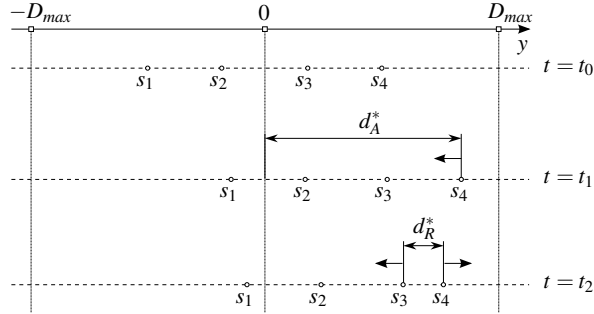
Fig. 8: Qualitative evolution of the cluster behaviour.

one-dimensional space is considered at three subsequent times $t_0 < t_1 < t_2$. At the initial time t_0 they are deployed in a configuration that satisfies a set of minimum and maximum distance constraints, and over time they move from the left to the right at a constant pace (this represents the orbital decay the spacecraft would be subject to). At time t_1 the object s_4 reaches a distance d_A^* from the origin, thus the smallest available impulse is provided in the negative direction to invert its motion and prevent it from reaching the border at $y = D_{max}$. The distance between s_4 and s_3 starts to shrink and when at time t_2 it reaches the value d_R^*, it induces s_4 and s_3 to fire in the positive and in the negative direction, respectively. A cascade effect is generated and over time all the objects perform small corrections.

It should be taken into account that an applied correction does not have an immediate effect, and the direction of the motion is altered with a delay up to one orbital period. This difference between the two frameworks derives from the employed control scheme, which is based on the Gauss Variational Equations [1]. To obtain a semi-major axis adjustment while leaving the other orbital elements unchanged, the correction must consists of two separate control actions, one at the perigee and one at the apogee of the orbit (see e.g., [4, 14]). Consider the situation at time t_2 of the given example applied to a cluster, i.e. with satellites s_3 and s_4 reaching a separation d_R^*, but assume that s_4 has not completed yet its first maneuver started at time t_1. It is not recommended to let the two satellites evaluate a maneuver to increase their separation because the object s_4 is not moving on its *official* orbit, but on a transfer orbit, thus a misleading maneuver would be computed. It is instead more appropriate to wait until the completion of the on-going maneuver of s_4, and only then compute the new maneuver to adjust the distance $d_{3/4}$. In this case, however, a larger consumption is expected, because by the time the two satellites start the new computation, they will have reduced their distance below the value d_R^*, so that the impulses returned by the APF will be larger than the minimum. Since the potentials have been built with the goal to provide larger impulses as the distances get closer to the boundaries, in general this delayed computation is not an issue, but it can become problematic depending on the specific set of inputs of the problem. The smaller the difference between the distances d^* and the correspondent distance boundary (D_{min} or D_{max}), the steeper the functions F, with an increase of the chances that the cluster keeping procedures fail.

Another aspect that needs to be considered is the differential consumption. In the one-dimensional example given through Fig. 8, it has been assumed that each object gives the same contribution when attempting to correct a relative behaviour, because for any pair of objects the reciprocal repulsion has always the same intensity and opposite direction. For a single correction, an equal consumption concerns the two involved objects, but on the overall the total consumption becomes unbalanced, because the shift of the cluster (due to the orbital decay) in the positive along-track direction induces the front object to perform more corrections than its follower, which performs more corrections than its follower, and so on. To contrast this behaviour Eq. (12) is modified into

$$\dot{y}_i = F_A(\Delta y_i) + \sum_{j=1, j \neq i}^{N} g_{i/j} F_R(\Delta y_{i/j}), \tag{31}$$

where the gains $g_{i/j}$ alter the contribution of the repulsion according to the remaining fuel masses. The gains are not based on the consumed mass because the satellites of the cluster are assumed to be heterogeneous, thus it is better to let those with more fuel perform more maneuvers rather than to enforce an equal consumption. Consider two objects A and B with the first having more fuel on board than the second. At any time, they exert on each other an equal repulsion, but by using Eq. (31), when they perform a maneuver to adjust their relative motion, A applies a correction larger than B, to compensate for the fact that B has a less fuel left on board.

Suppose now that the two objects are moving away from each other but it results $d_{A/B} < d_R^*$. This situation occurs, for example, right after the spacecraft apply a correction, because their distance requires some time to increase and to reach the inactivity region. In this case, there is no need for any of the spacecraft to perform an additional maneuver, but if the APF were only based on distances and masses, according to these information the algorithm would identify the need to increase the separation and would compute a new maneuver. To prevent such new computation, the direction of the relative motion, through the differential mean motion, is included into the evaluation of the gains $g_{i/j}$ and Eq. (31) is further modified into

$$\dot{y}_i = g_{i/0}F_A(\Delta y_i) + \sum_{j=1, j \neq i}^{N} g_{i/j}F_R(\Delta y_{i/j}), \qquad (32)$$

where the gain $g_{i/0}$ weights the attractive contribution by taking the motion of the spacecraft i with respect to the center into account.

4 Mission Scenarios

Different mission scenarios have been used to test the proposed method, which aims at performing cluster keeping for 50 days. All the performed simulations assumed a reference point with initial state $\text{œ}(t_0)$ as defined in Table 1, and a force field that encompasses the drag and the gravitational potential up to the term J_6. The distance

Table 1: Initial state of the reference point.

Element	Value	Units
semi-major axis - a	7000.92	km
eccentricity - e	0.01	
inclination - i	50.99	deg
RAAN - Ω	11.48	deg
argument of perigee - ω	19.12	deg
mean anomaly - M	21.00	deg

requirements and the number, initial distribution, and ballistic coefficients, of the satellites have been instead diversified among the simulations.

In each test, the initial configuration consists of randomly distributed spacecraft, with initial states obtained by applying Eqs. (1) and (6) to (8), to ensure that the distance constraints are satisfied. Two sets of distance boundaries have been used, a tight one $[D_{min,0} \ D_{max,0}]$ for the definition of the initial configuration, and a relaxed one $[D_{min} \ D_{max}]$ for the operational phase. The two sets are connected through

$$D_{min} = D_{min,0}(1 - \Delta_{min}) \qquad (33)$$

$$D_{max} = D_{max,0}(1 + \Delta_{max}), \qquad (34)$$

where the terms $[\Delta_{min} \ \Delta_{max}]$ express the percentage differences.

In the performed tests the proposed APF-based technique is applied to small sized clusters, for which Table 2 summarizes the configuration constraints (column DC_0), and the operational ones (column DC_{op}). A graphic representation of the

Table 2: Distance constraints.

Constraints	DC_0 [km]	DC_{op} [km]	Δ [%]
D_{min}	1	0.75	25
		0.50	50
D_{max}	5	6.25	25
		7.50	50

distance constraints is given instead in Fig. 9, which also introduces some codes to divide the entire pool of tests in smaller groups. The square at the bottom right
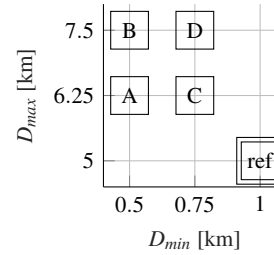
Fig. 9 Graphic representation of the distance constraints, along with the codes used to distinguish the various groups of tests.

corner highlights the set of configuration distances, while the four squares at the top left corner show the four sets of operational constraints and the code associated with the corresponding group of tests.

Concerning the activity/inactivity regions of the potentials, the values [0.25 0.5] have been tested for the parameter α_A, the values [0.5 0.75] for the parameter α_R.

Finally, as for the number N of spacecraft, clusters populated by 4, 6, 8, and 10 objects have been considered.

5 Reference Scenario

In this section a sample scenario is considered, to convey the idea of how the cluster evolves over time when the APF technique is applied. The inputs and parameters used in the test are outlined in Table 3. The cluster is initialized as depicted in

**Table 3:** Inputs and parameters for the sample case of cluster keeping.

Input	Value	Parameter	Value
N	6	α_A	0.5
$[D_{min,0}\ \ D_{max,0}]$	[1 km 5 km]	α_R	0.5
$[D_{min}\ \ D_{max}]$	[0.5 km 7.5 km]	β	25.89

Fig. 10, where an Earth-centered inertial frame is used. The solid and the dashed
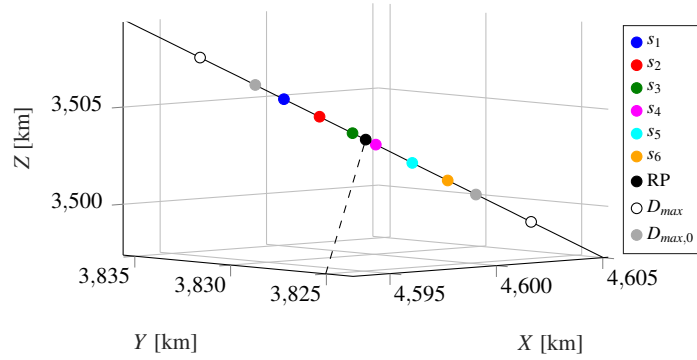
Fig. 10: Initial distribution of a sample test with $N = 6$ spacecraft.

lines denote the orbit of the RP and its position vector, respectively. The evolution of the relative distances can be observed in Figs. 11 and 12, the former showing the distances between the spacecraft and the center of the cluster, the latter displaying the distances between neighboring spacecraft. In both figures, together with the
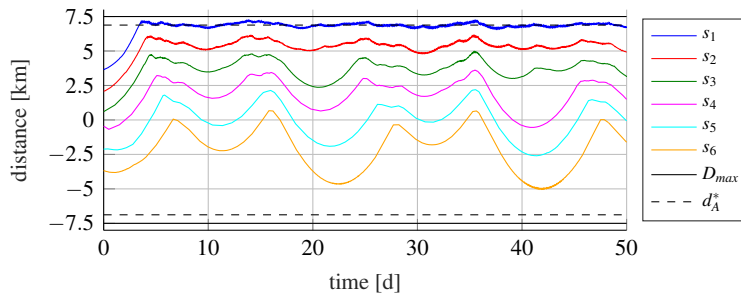

Fig. 11: Time evolution of the distances between the spacecraft and the RP.
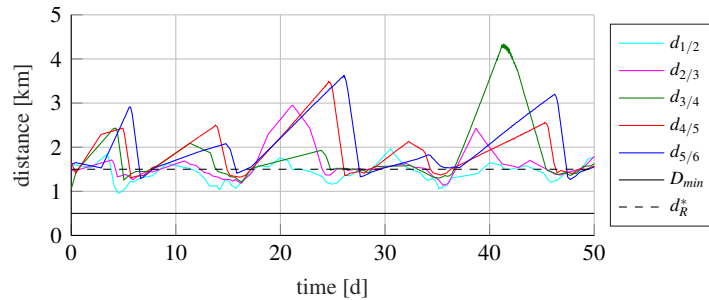
Fig. 12: Time evolution of the distances between neighboring spacecraft.

distances of interest, also the distance boundaries are reported, to give the reader a clear overview of the potentials activity regions. In Fig. 11, for which the distances

have been expressed in terms of the along-track coordinate y, it can be seen that the attraction significantly affects only the motion of the object s_1, since this is the only one exceeding the distance d_A^* from the center of the cluster. From Fig. 12, on the other hand, it can be noticed that all the spacecraft perceive repulsive contributions, as all the distances between neighboring objects decrease below the value d_R^*, thus entering the activity region of the repulsive potentials. For the correct interpretation of this figure, recall that the distance between the objects s_i and s_j is denoted as $d_{i/j}$.

Because of the drift of the cluster in the along-track direction caused by the orbital decay, a differential consumption can be observed with a Δv budget that decreases from the front to the rear of the cluster. The trend of the consumed mass over time is reported in Fig. 13 (it is worth mentioning that without the introduction of the gains $g_{i/j}$, the differential consumption would have been much more severe). Note that although the consumption trends increase monotonically, the thrust is not continuous. The figure refers to a time frame of 50 days, in which the satisfaction of the distance constraints is ensured through many frequent small impulsive actions. The black line represents an estimation of the mass consumption that would be re-
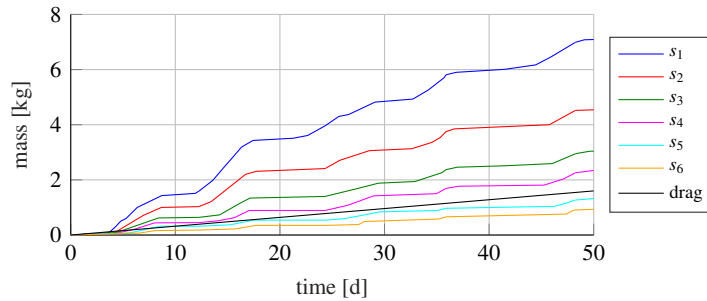

Fig. 13: Time evolution of the mass consumption.

quired to correct the effect of the drag. On average, the real recorded consumption is larger, but it is worth mentioning that the estimation is obtained by exploiting the analytical definition of the drag force, meaning that it entirely neglects the effect of the orbital decay, which is responsible for the drift of the mean anomalies and, in turn, of the cluster.

6 Simulation Results

This section summarizes the results obtained from the entire pool of simulations to give a general overview of the method behaviour.

In the first step it will be focused on the success of the method application and on how this can be related to the tuning parameters $[\alpha_A \ \alpha_R \ \beta]$, with the concept of success being associated with the satisfaction of the distance constraints. By assuming that the distance boundaries can be relaxed and that small violations can be tolerated,
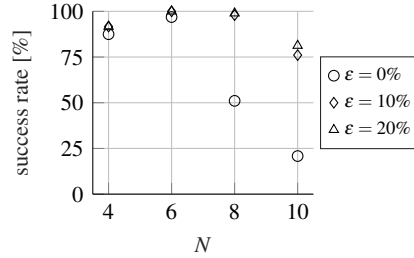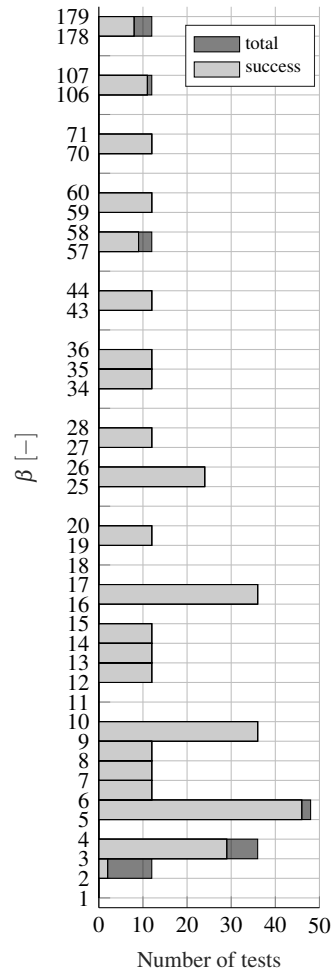
Fig. 14 Success rate of the cluster keeping as a function of the number of spacecraft.

an overview of the success rate as a function of the cluster density is given through Fig. 14, in which three thresholds ε have been used to identify acceptable violations.

The circular markers refer to the stricter conditions, in which no violations of the distance boundaries are accepted ($\varepsilon = 0\%$), while the diamonds and the triangles represent the success rates that would be obtained if violations up to 10% and 20%, respectively, could be tolerated. Note that even some of the triangular data remain below the 100% success rate, meaning that the entire pool contains also tests in which violations larger than 20% have been experienced (these tests are not further investigated and are associated with the failure of the method). Apart from the trivial result that larger tolerances involve higher success rates, what is interesting to see is that no significant difference exists between the trend of the diamonds and of the triangles, which means that if a violation occurs, it is either very small (the method is successful and the violations are within reasonable tolerance) or very large (the method fails). Concerning the cluster density, one would expect that a reduction in this parameter would increase the success rates, because a larger spacing between the objects involves wider regions of activity of the potentials, and thus flatter profiles of the F functions. This behaviour, however, is confirmed only when the number N of spacecraft is limited to the range [6 10], because for sparse clusters the low value of N requires large values of the ratio β, which increases the chances that too large corrections are performed and, in turn, that the method fails.

Figure 15 shows how the success rate changes with the value of the ratio β; all the results refer to the use of the largest tolerance $\varepsilon = 20\%$. The


Fig. 15: Success rate of the cluster keeping as a function of the ratio β.

lowest success rates are obtained in correspondence of the smallest and the largest values of β, with the worst results returned for $\beta < 4$. Small values of β produce profiles of the functions F that are too flat (the values F_{min} and F_{max} are very similar to each other), leading to a weak dependence from the distance. All the corrections provide Δv very similar to each other, and this does not always guarantee the satisfaction of the distance constraints. Large values of β correspond instead to large values of F_{max} and steep profiles of F, which can involve too large corrections and excessive semi-major axis differences. Since in each test the employed value of β was also its minimum allowed value β_{min} (smaller values would not yield the desired shape for the attractive and repulsive contributions U_A and U_R), when the profile of F is too flat, it can be assumed $\beta > \beta_{min}$ to reduce the chances that the method fails. On the contrary, in the case of steep profiles, it is not possible to adjust the value of β, because its reduction would not produce the desired shape. In these cases, one has to tweak the definition itself of the ratio β by changing the distance boundaries $[D_{min} \ D_{max}]$ and/or the parameters $[\alpha_A \ \alpha_R]$ that influence its evaluation.

As next step for the inspection of the method, the effect of the parameters α_A and α_R on the success rate has been considered. These parameters are responsible for the width of the activity/inactivity regions of the potentials and, together with the ratio β, for the steepness of the functions F. By applying the tolerance $\varepsilon = 20\%$ to identify the successful tests, the failure rate is approximately equal to 7%, with Fig. 16 showing how this rate can be divided according to the employed values of α_A and α_R. As expected, the smaller the activity region (large α_A, small α_R), the
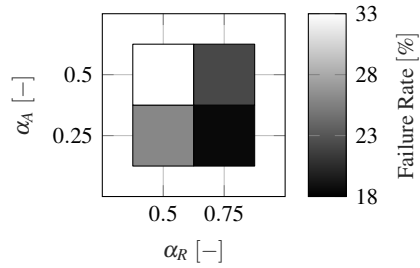

**Fig. 16** Failure rate associated with different $[\alpha_A \ \alpha_R]$ sets.

steeper the functions profiles, and the higher the chances that the method fails.

Figures 17 and 18 show the Δv budget and the number of control actions N_a required for the cluster keeping; each marker refer to an entire cluster, i.e. the depicted Δv and N_a are averaged over the entire population of spacecraft. None of the parameters change significantly with the set of operational constraints (for a given number N of spacecraft), but they both increase with the population of the cluster (for a given set of constraints), since the reduced relative separations require corrective maneuvers more frequently.

Finally, Figs. 19 and 20 focus on the violations of the minimum and maximum DC, showing how their frequency varies with their intensity, which is expressed in percentage terms with respect to the distance boundaries D_{min} and D_{max}. The recorded violations of the minimum distance boundary are spread in almost the entire range 0-20%, but an increase in their size corresponds to a reduction in their
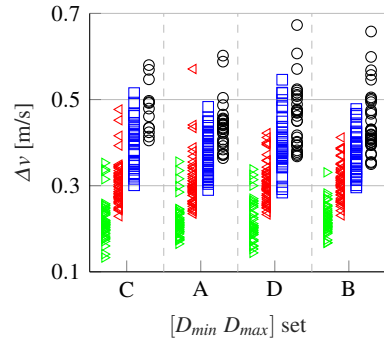
Fig. 17: Δv budget expressed as a function of the distance constraints ([A B C D]) and the number N of spacecraft (10 = ○, 8 = ◇, 6 = ◁, 4 = ▷).
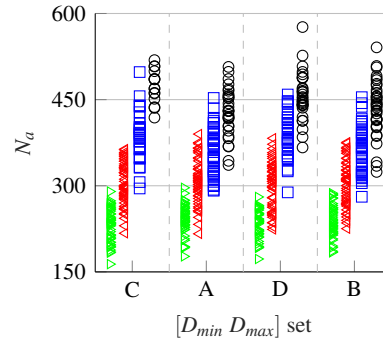
Fig. 18: Number of control actions expressed as a function of the distance constraints ([A B C D]) and the number N of spacecraft (10 = ○, 8 = ◇, 6 = ◁, 4 = ▷).
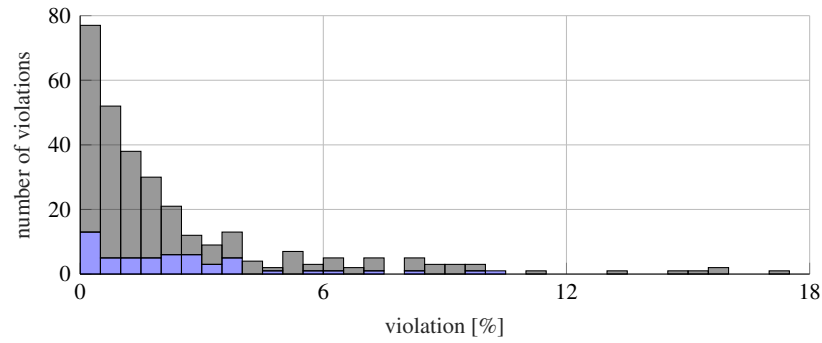
Fig. 19: Frequency vs intensity of the minimum distance constraints violations. Different colors refer to different numbers N of spacecraft (10 = ▬, 8 = ▬, 6 = ▬, 4 = ▬).
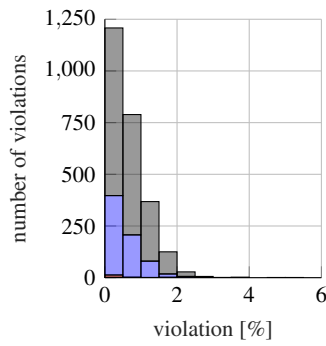
Fig. 20: Frequency vs intensity of the maximum distance constraints violations. Different colors refer to different numbers N of spacecraft (10 = ▬, 8 = ▬, 6 = ▬, 4 = ▬).

frequency, with large violations occurring only sporadically. In addition, the experienced violations decrease with the number of spacecraft N, and for the sparsest clusters ($N = 4$ and $N = 6$) they even reduce to zero. This behaviour was already anticipated, and can be attributed to the fact that an increase of the cluster density involves smaller relative separations, leading thus to higher chances for a violation to occur.

For what concerns the violations of the maximum distance constraints, it must be recalled that they relate only to the first spacecraft of the chain, due to the drift of the cluster in the positive along-track direction caused by the orbital decay. Once again an inverse relationship exists between the frequency and the size of the violations, but this time they are less severe and remain always below 6% of the D_{max} boundary; as a matter of fact, with reference to the unsuccessful tests, in the majority of the cases the APF application failed because the minimum distance boundary was critically violated, not the maximum distance boundary.

7 Conclusions

An artificial-potentials-based technique is proposed to perform cluster keeping. To guarantee a safe relative motion, the loose distance constraints and the large number of spacecraft that characterize a cluster scenario require new procedures, with respect to what is typically done in a formation. The control scheme does not have to maintain a precise relative configuration, but can simply react on the current one and modify it, if needed, while ensuring that the desired distance constraints remain satisfied. At the same time, to properly deal with the large amount of involved objects, the cluster keeping scheme should be autonomous and scalable. These features can be found in the technique of the artificial potentials, which can provide a simple and reactive guidance and control scheme, as it is only based on the current positions.

The proposed technique is tailored for clusters of spacecraft distributed in the along-track direction, so that their relative motion can be properly altered by just adjusting their semi-major axes, and in turn their mean motions. Through the use of the artificial potentials, the orbital corrections can be based on the sole current distance between the objects, and no orbital propagation or optimization schemes are required, paving the way for the on-board applicability of the algorithm. The proposed technique is not only real-time capable, but takes also the features of the propulsion system into account, thus including realistic limitations on the orbital corrections that can be performed by the spacecraft.

The provided results show the effectiveness of the proposed strategy.

References

[1] R. H. Battin. *An introduction to the mathematics and methods of astrodynamics, revised edition*. Ed. by J. S. Przemieniecki. AIAA education series. American Institute of Aeronautics & Astronautics, 1999.

[2] N. Bloise et al. "Obstacle avoidance with potential field applied to a rendezvous maneuver". In: *Applied sciences* 7.10, 1042 (2017), pp. 1–16.

[3] F. J. de Bruijn and E. Gill. "Delayed target tracking for along-track formations". In: *Journal of guidance, control, and dynamics* 38.7 (2015), pp. 1318–1323.

[4] F. Fumenti et al. "Quasi-impulsive maneuvers to correct mean orbital elements in leo". In: *Proceedings of the 3rd ceas eurognc*. Toulouse, France, 2015.

[5] V. Gazi and K. M. Passino. "Stability analysis of swarms". In: *Ieee transactions on automatic control* 48 (2003). APF, artificial potential function, pp. 692–697.

[6] V. Gazi and K. M. Passino. "A class of attractions/repulsion functions for stable swarm aggregations". In: *International journal of control* 77.18 (2004). apf, artificial potential functions, pp. 1567–1579.

[7] P. Gurfil and D. Mishne. "Cyclic spacecraft formations: relative motion control using line-of-sight measurements only". In: *Journal of guidance, control, and dynamics* 30.1 (2007), pp. 214–226.

[8] D. Izzo and L. Pettazzi. "Autonomous and distributed motion planning for satellite swarm". In: *Journal of guidance, control, and dynamics* 30.2 (2007), pp. 449–459.

[9] D. Izzo and L. Pettazzi. "Equilibrium shaping: distributed motion planning for satellite swarm". In: *Proc. 8th intern. symp. on artificial intelligence, robotics and automation in space*. 2005.

[10] J. Luo et al. "Consensus of satellite cluster flight using an energy-matching optimal control method". In: *Advances in space research* 60.9 (2017), pp. 2047–2059.

[11] N. Martinson. "Obstacle avoidance guidance and control algorithm for spacecraft maneuvers". In: *Aiaa guidance, navigation, and control conference*. AIAA 2009-5672. Chicago, Illinois, 2009.

[12] L. Mazal and P. Gurfil. "Cluster flight algorithms for disaggregated satellites". In: *Journal of guidance, control, and dynamics* 36.1 (2013), pp. 124–135.

[13] L. Mazal and P. Gurfil. "Closed-loop distance-keeping for long-term satellite cluster flight". In: *Acta astronautica* 94.1 (2014), pp. 73–82.

[14] H. Schaub and K. T. Alfriend. "J_2 invariant relative orbits for spacecraft formations". In: *Celestial mechanics and dynamical astronomy* 79.2 (2001), pp. 77–95.

[15] M. Schlotterer and S. Novoschilov. "On-ground path planning experiments for multiple satellites". In: *23rd international symposium on space flight dynamics 2012*. 2012.

[16] M. Schlotterer et al. "On-ground testing of autonomous guidance for multiple satellites in a cluster". In: *8th international workshop on satellite constellations and formation flying*. 2015.

[17] S. Wan et al. "Hybrid approach to optimize the cluster flying orbit for fractionated spacecraft based on PSO-SQP algorithm". In: *2nd international conference on systems engineering and modeling (ICSEM-13)*. 2013.

[18] J. Wang and S. Nakasuka. "Cluster flight orbit design method for fractionated spacecraft". In: *Aircraft engineering and aerospace technology: an international journal* 84.5 (2012), pp. 330–343.

[19] H. Zhang and P. Gurfil. "Distributed control for satellite cluster flight under different communication topologies". In: *Journal of guidance, control, and dynamics* 39.3 (2016), pp. 617–627.

[20] H. Zhang and P. Gurfil. "Satellite cluster flight using on-off cyclic control". In: *Acta astronautica* 106 (2015), pp. 1–12.